ATLAS NOTE

June 26, 2009

Reconstruction of High Mass $t\bar{t}$ Resonances in the Lepton+Jets Channel

The ATLAS Collaboration

ATL-PHYS-PUB-2009-081
26 June 2009

Abstract

At the LHC, highly energetic pp collisions are expected to be the source of new experimental phenomenology. Top quarks will notably be produced with high transverse momenta for the very first time, leaving in the detector an unusual signature. Indeed, hadronic top quark decay products can be so close together in the detector that they are reconstructed as a single jet, and semi-leptonic top quark decays can no longer count on the presence of a truly isolated lepton for their identification. This note describes the use of new experimental techniques in the identification of these objects as part of a realistic analysis for a high mass $t\bar{t}$ resonance search with the ATLAS detector.

1 Introduction

At the Large Hadron Collider (LHC) at CERN, where proton-proton collisions will occur at an unprecedented energy of $\sqrt{s} = 14$ TeV and high luminosity of 10^{34} cm^{-2}s^{-1}, particle physics will enter a new phase. The characteristics of the LHC will not only allow for precise measurements of the Standard Model parameters but will probably also open a window onto new physics phenomena and thus provide first tests of some *Beyond the Standard Model* theories.

With these technological advances come new challenges for experimental particle physics. Indeed, massive objects (at the electroweak scale) will be produced abundantly and with large transverse momenta at the LHC, modifying significantly their decay signatures in the detector. In this context, the top quark will be a major source of such new experimental phenomenology. At low to moderate transverse momentum, a top quark that decays hadronically ($t \to bq\bar{q}$) allows for a reconstruction method that relies on the identification of three jets (a b-jet and two light quark jets) whereas the reconstruction of a top quark decaying semi-leptonically ($t \to bl\nu_l$) relies on the identification of a b-jet, an isolated lepton and some missing transverse energy due to the neutrino (see Fig. 1). However, highly boosted tops will leave a very different signature in the detector, thus the need for novel identification methods.

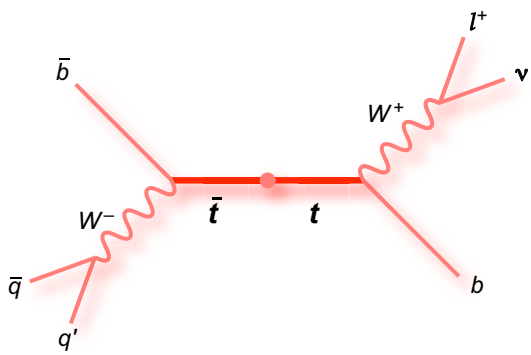

Figure 1: Schematic illustration of a l+jets $t\bar{t}$ event.

Hadronically decaying top quarks with very large transverse momenta provide a good example of this new experimental phenomenology. Indeed, the top quark decay products ($bq\bar{q}$) can be so close together in the detector that they cannot be distinguished from each other and are thus reconstructed as a single jet: a *monojet*. As for highly boosted semi-leptonic top decays, the difference lies in the fact that the lepton is no longer isolated. This is a major concern for electronic top decays ($t \to be\nu_e$) where the electron from the W boson decay can be so close to the resulting b-jet that the full electron energy is often counted in the jet energy.

The aim of this study is to perform high mass $t\bar{t}$ resonance reconstruction using a new approach in the identification and reconstruction of high-p_T top quarks. "ℓ + jets" $t\bar{t}$ decays are investigated requiring the identification of both a hadronic top monojet ($t \to bq\bar{q}$) and a high-p_T semi-leptonic top ($t \to be\nu_e$ or $t \to b\mu\nu_\mu$) where the lepton is not isolated. The identification of hadronic monojets is done using the method described in Ref. [1]. The focus of this note is on the rejection of QCD multijet background. In the search for resonances, discrimination against the irreducible $t\bar{t}$ background has to come from improving the $t\bar{t}$ mass resolution, which is the topic of an ongoing study. A semi-quantitative discussion of non-$t\bar{t}$ W boson + jets background is included in section 5.

2 Monte Carlo Data Sets

Datasets used in this study are all simulated using a GEANT-based [2, 3] description of the ATLAS detector, and reconstructed using the standard ATLAS reconstruction algorithms. pp collisions with

center-of-mass energy of 14 TeV are taken as the starting point. Both signal and multijet background samples are produced using the PYTHIA [4] event generator. Signal samples are $Z' \to t\bar{t}$ events, where the standard model-like Z' bosons have a mass of 2 and 3 TeV. In these events, one of the W bosons from top quark decays is forced to decay hadronically, and the other to an electron or a muon. Background samples are QCD multijet samples with 280 GeV $< p_T <$ 560 GeV (σ = 12.5 nb), 560 GeV $< p_T <$ 1120 GeV (σ = 0.35 nb) and 1120 GeV $< p_T <$ 2240 GeV (σ = 6 pb) respectively[1)]. The irreducible $t\bar{t}$ continuum background is evaluated by application of the top quark reconstruction efficiencies to MC@NLO [5, 6] and PYTHIA generator-level events. Except as otherwise noted, jets used throughout this study are reconstructed using the $k_\perp$ algorithm with $D = 0.6$.

The performance of standard ATLAS reconstruction algorithms on fully simulated events processed with the same software version is extensively documented in Ref. [7].

3 Reconstruction of Semi-leptonic Top Quark Decays

3.1 Muonic Top Quark Decays

The preselection of muons is as follows:

- $p_T > 20$ GeV,
- matching tracks in the muon system and inner detector, and
- $|\eta| < 2.5$,

where η is the muon pseudorapidity.

At least one jet with $p_T > 200$ GeV is then required to lie in a cone of radius $R = \sqrt{(\Delta\eta)^2 + (\Delta\phi)^2} = 0.6$ (with ϕ the azimuthal angle) centered on the hardest muon of the event. The closest of these jets is assumed to be the b-jet and the muon is labeled as coming from the W boson decay. We refer to this system (selected muon and the candidate b-jet) as a muonic top.

This loose selection of muonic tops is subject to a lot of fake identifications in a ℓ+jets $Z' \to t\bar{t}$ sample. Indeed, the wrong muon (coming from one of the two b-jets) and/or the wrong jet may be selected, forming a fake muonic top. This tendency for fake identification is in fact prominent with low p_T reconstructed muons, but instead of making a drastic cut on the p_T of the reconstructed muon, two new variables, which give more insights on real muonic tops and thus better discrimination from fakes, are introduced.

The first of these variables is taken from Ref. [8] and measures the fraction of (visible) mass of the top carried away by the muon:

$$x_\mu \equiv 1 - m_b^2/m_{visible}^2,$$

where m_b is the mass of the candidate b-jet and $m_{visible}$ is the visible mass of the muonic top ($b + \mu$.) For leptonic tops [8] the invariant mass of the resulting b-jet is expected to be around 10% of m_t and x_μ is peaked towards 1. The other variable is defined as the p_T of the muon with respect to the candidate b-jet, times the angle (in η, ϕ space) between the muon and the candidate b-jet:

$$y_\mu \equiv p_{\mu\perp b} \times \Delta R(\mu, b).$$

As such, it is similar to the (square root of the) $k_\perp$ distance defined in the $k_\perp$ jet clustering algorithm. It is expected that selected muons that come from fakes will have a small value of y_μ.

Figure 2 shows the 2-d distributions of (x_μ, y_μ) for true and fake muonic tops. In order to reduce the percentage of fake muonic tops coming out of the loose selection described above, we require that $y_\mu > (-40x_\mu + 20)$ GeV. This 2-d cut in (x_μ,y_μ) space is also efficient to reject fake muonic top candidates preselected in QCD multijet samples as shown in Fig. 3.

[1)] In this context, p_T denotes the `CKIN(3), CKIN(4)` parameters in PYTHIA.

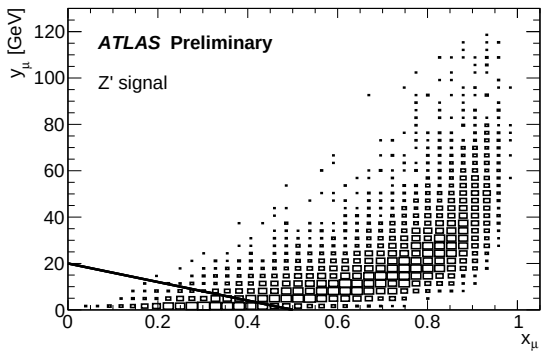

(a)

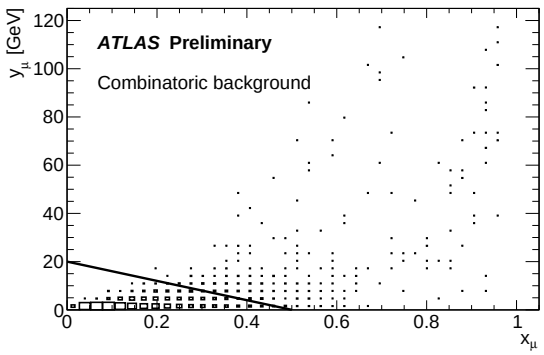

(b)

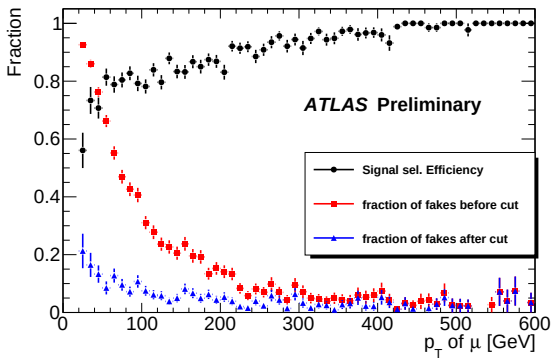

(c)

Figure 2: Fake rejection for muonic tops in l+jets $Z' \to t\bar{t}$: a) 2-d distributions of x_μ, y_μ for real muonic tops: selected events are required to lie above the line; b) 2-d distributions of x_μ, y_μ for fake muonic tops: selected events are required to lie above the line; c) Selection efficiency for real muonic tops (circles) and fraction of fake muonic tops w.r.t. all preselected events in the signal sample before (squares), and after (triangles) the cut.

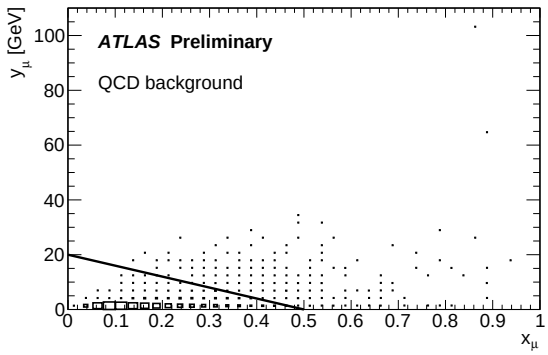

(a)

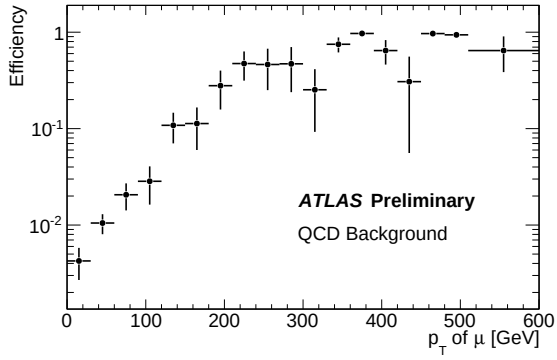

(b)

Figure 3: Muonic top candidates in QCD multijet samples: a) 2-d distributions of x_μ, y_μ. Selected events are required to lie above the line; b) Selection efficiency of the 2-d cut after preselection.

3.2 Electronic Top Quark Decays

The preselection of electrons is as follows:

- $p_T > 20$ GeV,
- an electron-like shower shape (following the "medium" selection in [7]), and
- $|\eta| < 2.5$ while excluding the crack region between the barrel and endcap calorimeters ($1.37 < |\eta| < 1.52$).

The selection of electronic top quark decays needs to be tackled in a slightly different way than their muonic counterparts. Thanks to the fine granularity of the ATLAS calorimeters, electrons can be reconstructed with good efficiency even if embedded in jets. In this case, the full electron energy is often counted in the jet energy. Therefore, a jet with $p_T > 300$ GeV is required to lie in a cone of radius $R = 0.6$ centered on the hardest electron of the event. Furthermore, in this search for a high p_T jet (the candidate b-jet) neighboring the electron, we systematically reject jets with a first $k_\perp$ splitting scale[2)] smaller than 10 GeV to eliminate the few cases where the electron energy is not included in the jet. With these requirements, a negligible proportion of fake electronic tops are selected in $Z' \to t\bar{t}$ samples and so, we will focus here on background (QCD multijet) rejection.

In complete analogy with the muonic case, we define the variables x_e and y_e where, the working hypothesis being that the b-jet and the electron are merged in a single jet (which is mostly the case in the sample of signal events), care is taken to subtract the electron's four-momentum from the selected jet to *extract* the b-jet. It was also found to be useful to introduce a new variable,

$$y'_e \equiv p_{e\perp j} \times \Delta R(e, j),$$

where the j refers to the selected jet (i.e.: without subtracting the electron). The proposed cuts are $y'_e > 1$ and $y_e > (-40x_e + 20)$ GeV, as shown in Fig. 4.

3.3 Neutrinos

All missing transverse energy of the event is assumed to come from the neutrino of the semi-leptonic top decay. We ask for $E_T^{miss} > 20$ GeV and the z-component of the neutrino's momentum is deduced from the W boson mass constraint using the previously identified lepton. If two real solutions are found for p_z^ν, which happens 74% of the time in the signal, we take the one with the smallest value of $|p_z^\nu|$; this choice is correct, in the sense that the solution closest to the real p_z^ν is picked, 60 % of the time. (Choosing the p_z^ν solution closest to p_z^ℓ is correct 51% of the time.) If on the other hand no real solution is found (because we might overestimate the neutrino's transverse momentum by using all E_T^{miss}), only the real part of the complex solutions is considered. Once p_z^ν is fully determined, we further require that $\Delta R(\nu_l, l) < 1$ in an attempt to reject misreconstructed neutrinos, as we expect the decay products of the W boson to be collimated. This last cut has a very small effect ($> 95\%$ selection efficiency) on the neutrino candidates for which the W boson mass constraint yields two real solutions for p_z^ν, but it does exclude 46% of the neutrino candidates where no real solutions was found for p_z^ν.

3.4 Summary of the Leptonic Top Quark Selection Procedure

A brief summary of the procedure followed for selecting leptonic tops in $Z' \to t\bar{t}$ samples is presented here for the sake of clarity:

- Identify candidate muonic top

[2)] See Sect. 4.1.1 for more details on $k_\perp$ splitting scales.

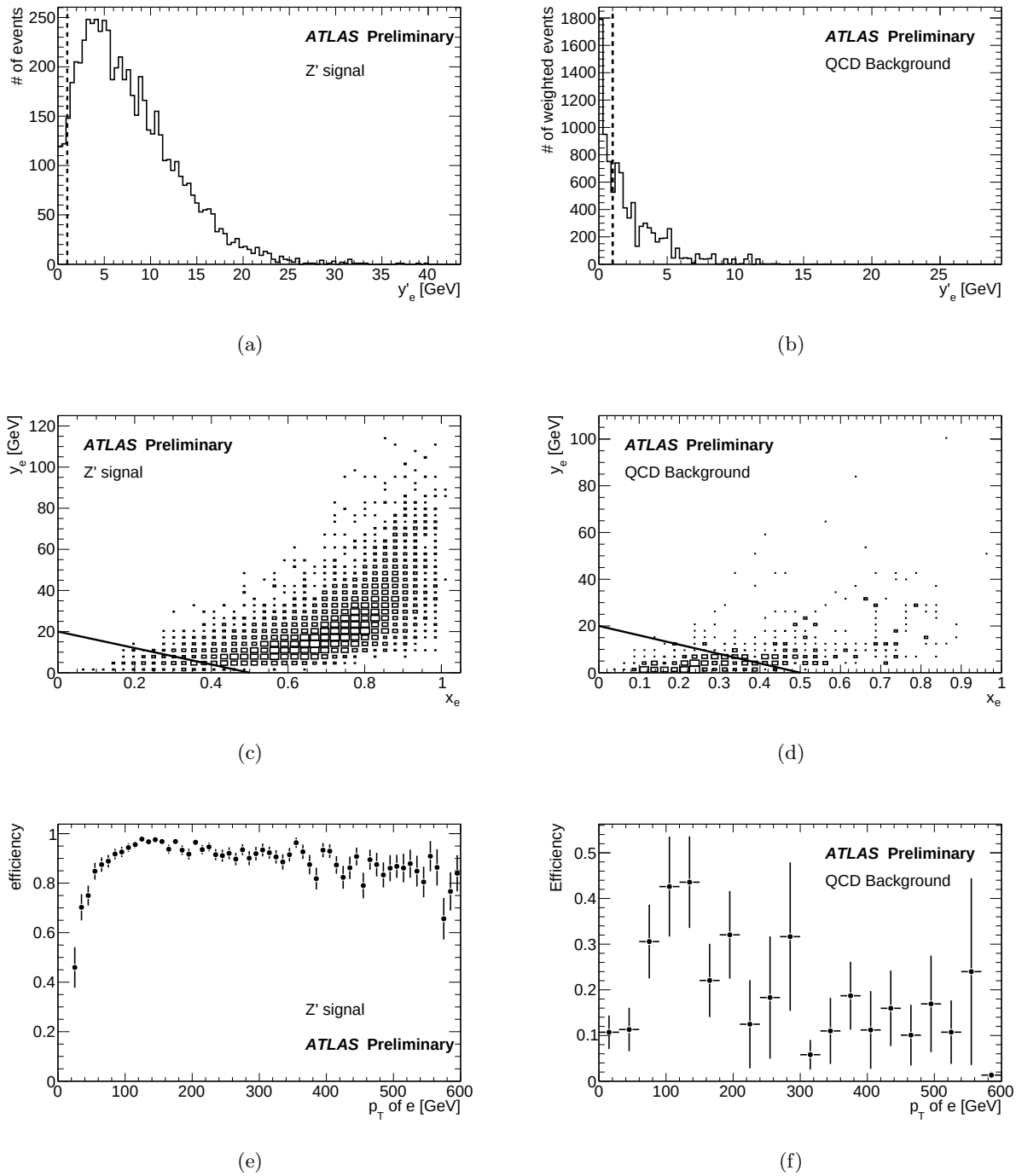

Figure 4: Electronic top quark decays: a) y'_e distribution for signal. (The dashed line indicates the cut.) b) y'_e distribution for QCD multijet background. c) 2-d distributions of x_e, y_e for electronic tops after the cut on y'_e: selected events are required to lie above the line. d) 2-d distributions of x_e, y_e for electronic top candidates from QCD multijet samples after the cut on y'_e: selected events are required to lie above the line. e) Selection efficiencies of the proposed cuts for signal, and f) Selection efficiencies of the proposed cuts for QCD background after preselection.

1. Select hardest reconstructed muon (passing the preselection cuts) in the event.
2. Require a close jet ($\Delta R(j, \mu) < 0.6$) and if found, require this system ($j + \mu$) to pass 2-d

cuts on the variables x_μ and y_μ.

- Identify candidate electronic top
  1. Select hardest reconstructed electron (passing the preselection cuts) in the event.
  2. Require a close jet ($\Delta R(j,e) < 0.6$) with $k_\perp$ splitting scale larger than 10 GeV and if found, require this jet ($j = b+e$, the hypothesis being that the electron is part of the reconstructed jet) to pass cuts on the variables x_e , y_e and y'_e.
- If in an event we find both a muonic and an electronic top candidate, select the one with the hardest lepton.
- Add the neutrino to the selected *visible* leptonic top by using the W boson mass constraint and require that $\Delta R(\nu_l, l) < 1$.

4 Reconstruction of Hadronic Top Monojets

With the full leptonic top in hand, we aim at identifying a hadronic top monojet in the event. The highest p_T jet (which does not coincide with the leptonic top) with a p_T of at least 300 GeV (so that the top decay products are collimated enough to be reconstructed as a single jet) is the natural candidate. However, with background rejection in mind, we make further requirements on this candidate top monojet.

4.1 Likelihood Variable

Four variables are considered in the construction of a likelihood variable for hadronic top monojets. These are introduced in Refs. [9,1,7] and are the first three $k_\perp$ splitting scales and the jet mass. The procedure followed in the present study to obtain these $k_\perp$ splitting scales will first be briefly outlined.

4.1.1 $k_\perp$ Splitting Scales

This analysis uses $k_\perp$ jets with $D = 0.6$. We are interested in the energy scales at which such jets splits into 2, 3 or 4 subjets. To obtain these splitting scales, "topoclusters"[3)] are taken as the jets' constituents and fed to FastJet [10] for reclustering by means of the $k_\perp$ algorithm. FastJet provides a simple method to extract the $k_\perp$ splitting scales (also called d_{min} values): $d_{min(n,n+1)}$ is the minimal $k_\perp$-distance corresponding to the recombination from $n+1$ subjets to n subjets. As such, the square root of $d_{min(1,2)}$ ($d_{min(2,3)}$, $d_{min(3,4)}$) corresponds to the characteristic energy scale at which a jet splits into 2 (3 , 4) subjets.
We thus define the first three $k_\perp$ splitting scales as $\sqrt{d_{min(1,2)}}$, $\sqrt{d_{min(2,3)}}$ and $\sqrt{d_{min(3,4)}}$ [4)].

4.1.2 Construction

We construct a likelihood ratio for each jet i as:

$$y_L(i) = \frac{\ln\left(L_S(i)/L_B(i)\right)}{15} \tag{1}$$

[3)] topoclusters [7] are built based on a topological clustering algorithm that groups cells in clusters based on their neighbor relations and on the significance of their energy contents, exploiting the fine granularity of the ATLAS calorimeters to reduce sensitivity to noise and pile-up.

[4)] To be more precise, we define the $k_\perp$ splitting scales as $\epsilon\sqrt{d_{min(1,2)}}$, $\epsilon\sqrt{d_{min(2,3)}}$ and $\epsilon\sqrt{d_{min(3,4)}}$, where ϵ is an energy scale correction factor (close to unity) which is the energy ratio of the original jet (calibrated after clustering) over the associated reclustered one (where the constituents themselves are first calibrated). See Ref. [1].

where

$$L_{S(B)}(i) = \prod_{k=1}^{n_{var}} p_{S(B),k}(x_k(i)). \tag{2}$$

Here $p_{S(B),k}$ is the signal (background) normalized probability density function of the kth variable, and 15 is an arbitrary normalization factor.

The *pdf*s are estimated for signal from top monojets in $Z' \to t\bar{t}$ samples (2 and 3 TeV Z' boson) and for background from jets in the QCD multijet samples. The exact procedure is as follows:

- For each input variable (which are the first three $k_\perp$ splitting scales and the jet mass) , smooth out both signal and background distributions.
- Fit these smoothed histograms to polynomial interpolation functions (cubic splines in this case) to obtain continuous *pdf*s for both signal and background.
- *pdf*s are saved in finely binned histograms and normalized to unity.

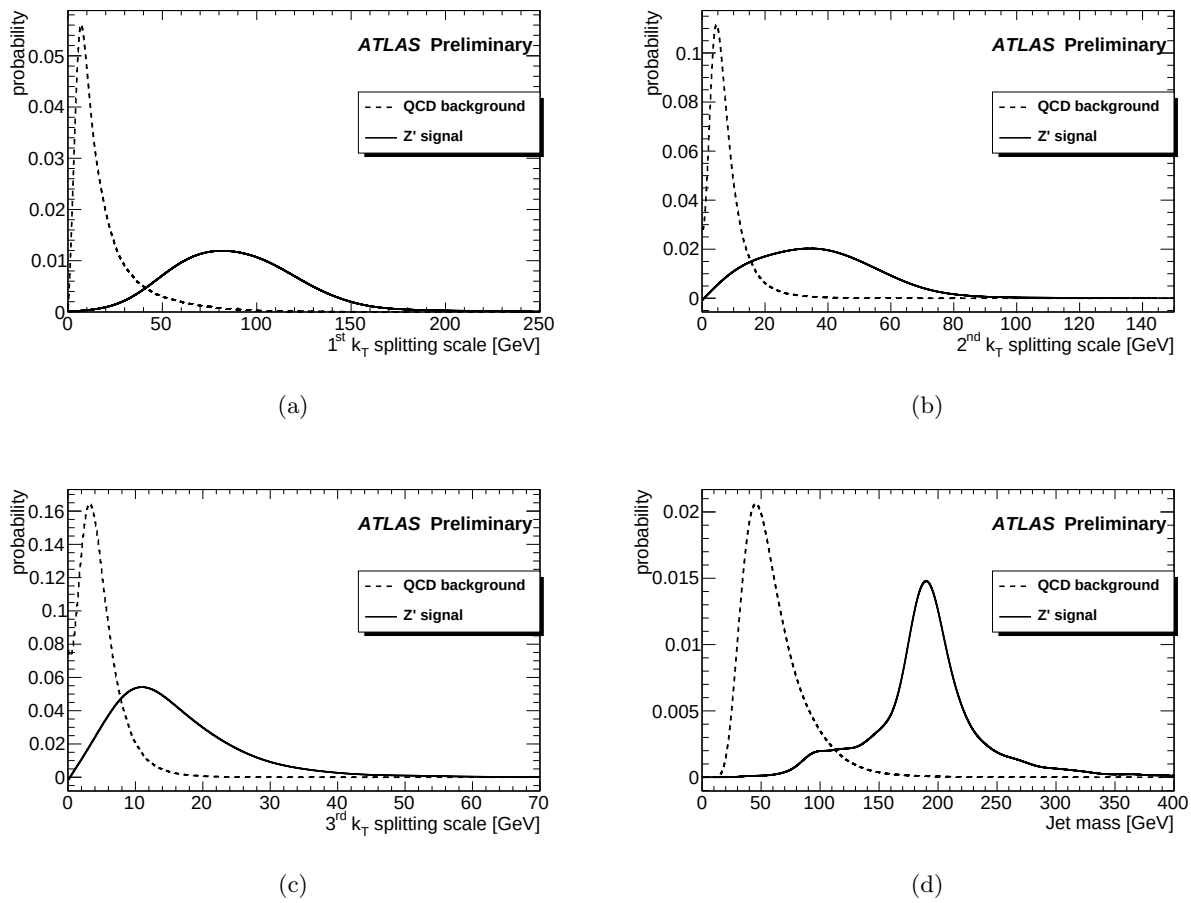

Figure 5: Normalized *pdf*s: a) 1st $k_\perp$ splitting scale for signal (plain line) and background (dashed line); b) 2nd $k_\perp$ splitting scale for signal (plain line) and background (dashed line); c) 3rd $k_\perp$ splitting scale for signal (plain line) and background (dashed line); d) Jet mass for signal (plain line) and background (dashed line).

Normalized smoothed *pdf*s for both signal and background are shown in Fig. 5 and the likelihood variable distributions as a function of jet p_T are shown in Fig. 6 with the selection efficiency for $y_L > 0.6$.

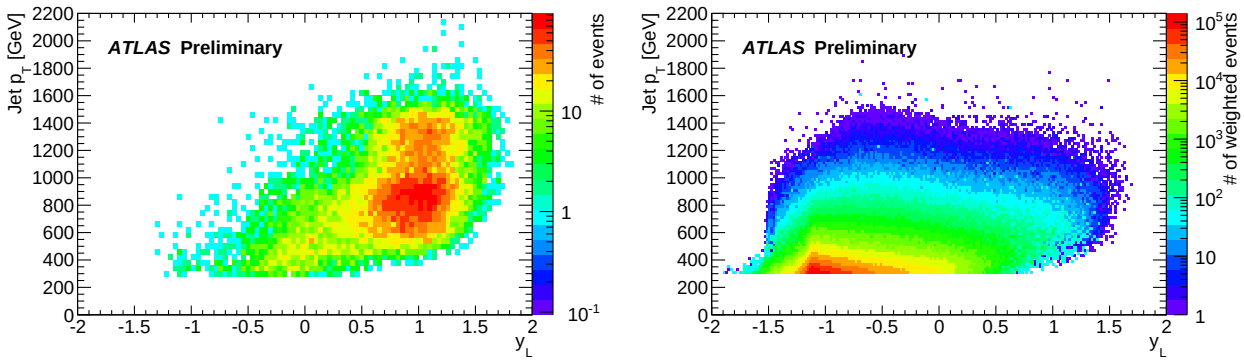

(a) (b)

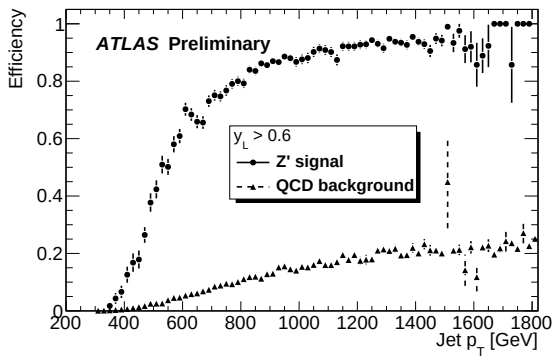

(c)

Figure 6: Likelihood distributions and selection efficiency (as a function of jet p_T) for hadronic top monojets: a) Jet p_T versus likelihood variable y_L for signal; b) Jet p_T versus likelihood variable y_L for background; c) Selection efficiencies for a likelihood cut ($y_L > 0.6$).

This simple approach in the construction of the likelihood variable y_L, optimal if the different variables are all independent, may not yield the most optimized cut in this case, but it has the advantage of simplicity. Furthermore, the correlation between the various variables for both signal and background is relatively small.

The candidate hadronic top monojet identified in the event is required to have $y_L > 0.6$.

5 Z' Boson Mass Reconstruction and Sensitivity

The Z' boson mass is reconstructed by simply adding the four-momentum of the selected semi-leptonic top and hadronic top monojet. It appears, as shown in Fig. 7 (dashed distributions), that this straightforward procedure yields mass distributions that are shifted to lower values than generated, especially for the $m = 3$ TeV Z' boson. Since at this time the jet energy is calibrated to the corresponding truth jet energy, we investigate if this can be improved by including out-of-cone energy: for each selected object, the ($k_\perp$) jet initially considered is replaced with the closest cone jet to which (calibrated) topoclusters located in a ring with inner radius of $R = 0.7$ and outer radius of $R = 1.2$ are added. The addition of these energy contributions leads to the reconstructed Z' boson masses shown in solid lines in Fig. 7.

In order to check that these additional energy contributions are not due to some detector artefact, calorimeter energy in a cone of $R = 0.4$, located far from the two top candidates (where there should

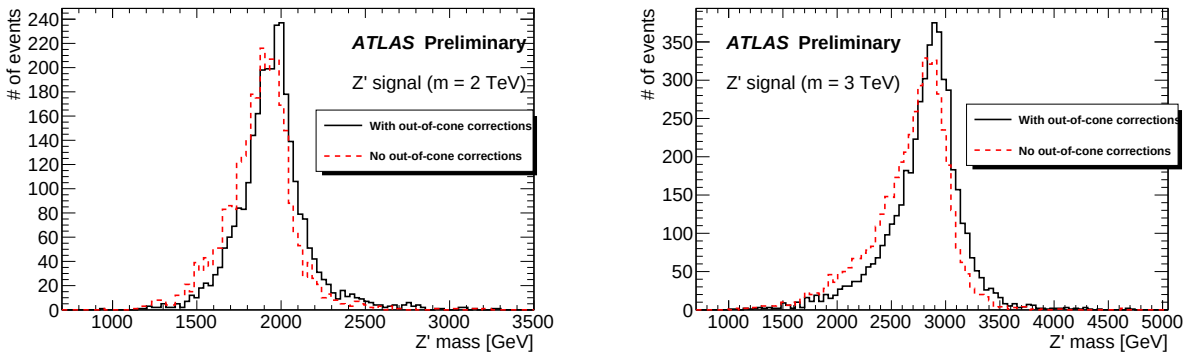

(a) (b)

Figure 7: Z' boson mass reconstruction with (solid) and without (dashed) the addition of energy contributions in rings around the selected top candidates for $m_{Z'} = 2$ (a) and 3 (b) TeV.

be no real signal), has been compared to the energy found in the rings around the top candidates. It was found that roughly 30% of the time, no protojets were found in this $R = 0.4$ cone. In the other 70% of the cases, we scaled the energy in the cone by the area in (η, ϕ) space to compare with the rings around the top candidates. The result is shown in Fig. 8. The difference between the distributions indeed suggests that a substantial fraction of the out-of-cone energy originates from the signal.

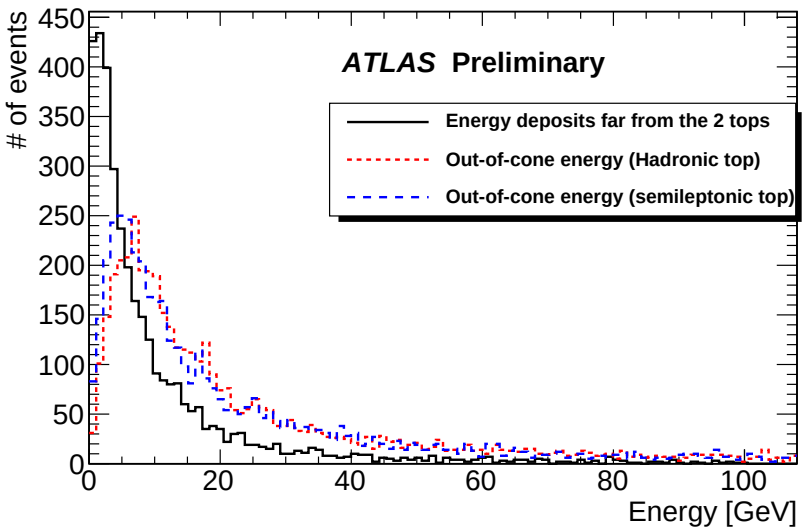

Figure 8: Comparison of energy deposits for the Z' boson sample ($m = 3$ TeV). Short-dashed line is the energy in a ring around the hadronic top monojet, the long-dashed line in a ring around the leptonic top and the solid line, in a cone away from the two tops. For the solid line, entries at zero have been suppressed (see text).

5.1 Mass Resolution

To determine the resonance mass resolution, the difference between the generated and the reconstructed mass (with the corrections described in the previous section) is plotted in Fig. 9 . The peak

of these distributions is fitted with a single gaussian. We observe a systematic shift of 44 GeV and a width of 98 GeV for the $m = 2$ TeV Z' boson. For the $m = 3$ TeV Z' boson, a systematic shift of 93 GeV and a width of 154 GeV is observed. More work to improve the mass resolution is underway.

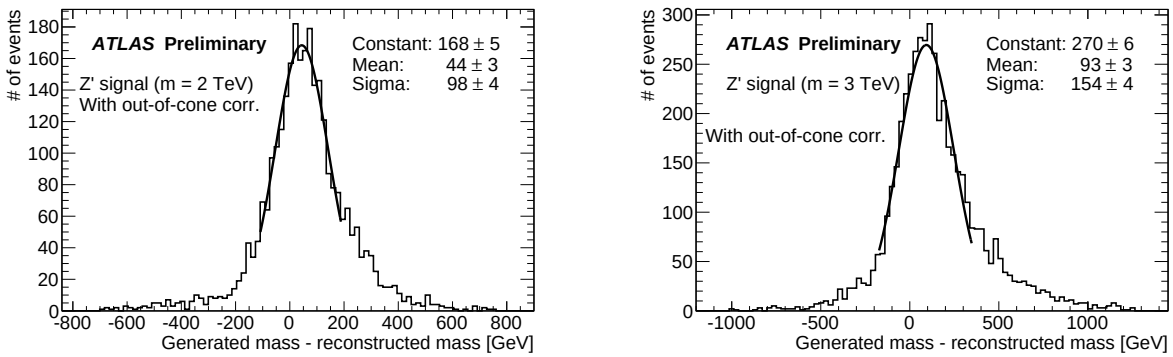

(a) (b)

Figure 9: Distribution of the generated mass minus the reconstructed mass for the $m = 2$ (a) and 3 (b) TeV Z' boson.

5.2 Total Selection Efficiency

Total selection efficiencies, based on the selection of one hadronic top monojet and one leptonic top, are estimated for both signal and background. For the $Z' \to t\bar{t}$ samples (m =2 and 3 TeV), efficiencies are shown in Figs. 10 and 11 as a function of the p_T of the leading jet in the selected event and for different values of the hadronic top monojet likelihood cut. Efficiencies are calculated w.r.t. all events in the samples and, to illustrate the effect of the selection cuts, also w.r.t. events where all required objects (two high p_T jets, missing transverse energy, lepton) were successfully reconstructed.

Total selection efficiencies for background are shown in Fig. 12 and are estimated in a different way due to the lack of sufficient statistics. The selection efficiency for the leptonic top was calculated for all events in the QCD multijet samples independently of the hadronic top monojet selection. The efficiency of the latter was also calculated for all QCD events (and for different values of the likelihood cut) and multiplied on a jet-p_T bin basis by the selection efficiency of the leptonic top to yield the total efficiency.

5.3 Expected Results For 1 fb^{-1} of Data

In order to appreciate the discriminating power of the selection cuts that are put forward in this study in a more realistic context, the number of expected events that survives the cuts for QCD multijet and standard model $t\bar{t}$ backgrounds for 1 fb^{-1} of data are presented in Table 1. Table 2 lists the signal selection efficiencies for various choices of the likelihood cut. In these tables, events are selected in a mass window of $[\overline{m}_{reco} - \sigma_{m_{reco}}, \overline{m}_{reco} + \sigma_{m_{reco}}]$ where $\overline{m}_{reco}$ is the mean and $\sigma_{m_{reco}}$, the standard deviation, obtained by fitting a gaussian to the central part of the reconstructed signal mass distribution. This corresponds to a mass window of $[1800, 2100]$ GeV for the $m = 2$ TeV Z' boson signal sample and $[2700, 3100]$ GeV for the $m = 3$ TeV Z' boson.

The QCD multijet samples are combined according to their cross-section to reflect 1 fb^{-1} of data: each event receives a weight of σ_{Jx}/N_{Jx}, where σ_{Jx} is the cross-section (in fb) and N_{Jx} is the number of generated events in sample Jx. To calculate the invariant mass of the system formed by the leptonic top and hadronic top monojet candidates in the QCD multijet background, the highest p_T jet in events passing the leptonic top selection (other than the selected leptonic top candidate) is assigned to be

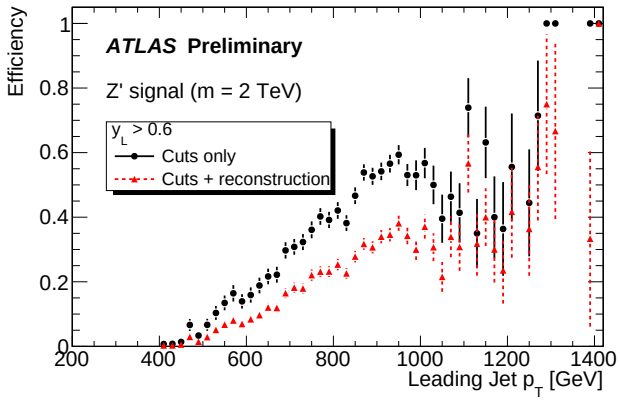

Figure 10: Total selection efficiency ($m = 2$ TeV Z' boson) as a function of leading jet p_T requiring $y_L > 0.6$. In this plot, circles and plain error lines are efficiencies w.r.t. events where all required objects are reconstructed, triangles and dashed error lines are efficiencies w.r.t. all events in the sample.

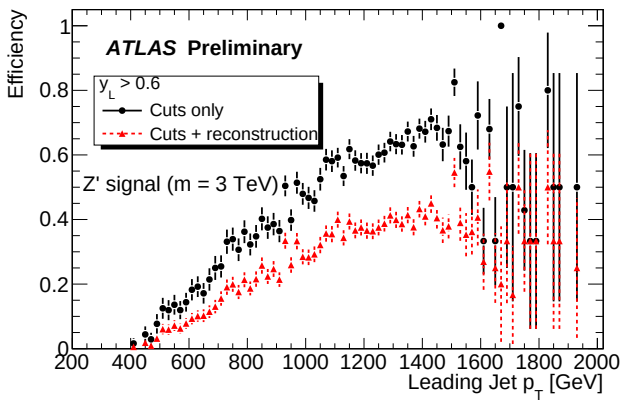

Figure 11: Total selection efficiency ($m = 3$ TeV Z' boson) as a function of leading jet p_T requiring $y_L > 0.6$. In this plot, circles and plain error lines are efficiencies w.r.t. events where all required objects are reconstructed, triangles and dashed error lines are efficiencies w.r.t. all events in the sample.

the hadronic top monojet candidate. These events are then weighted with the selection efficiencies of the hadronic top monojet likelihood cut (as a function of the leading jet p_T of the event).

The expected number of selected events coming from the standard model $t\bar{t}$ background is estimated by a different method because no appropriate (that is, with enough statistics) samples were available at the time of writing. Cross-sections of SM semi-leptonic $t\bar{t}$ decays with generated mass $m_{t\bar{t}}$ restricted to mass windows around 2 and 3 TeV are obtained with MC@NLO and then scaled to the NLO+NLL theoretical total cross-section of 833 pb. An 18% systematic uncertainty is assumed for these cross-sections, based on 10% from the uncertainty on the total cross-section $\oplus$ 15% because we extrapolate from a restricted area in phase space. The latter uncertainty was evaluated from a generator-level comparison between the PYTHIA and MC@NLO $m_{t\bar{t}}$ spectra with the total cross-section for both generators rescaled to 833 pb. We have taken half the difference as an estimator of the uncertainty. In order to obtain the approximate number of selected events, each SM $t\bar{t}$ event receives a weight corresponding to the reconstruction and selection efficiencies for the signal as a function of

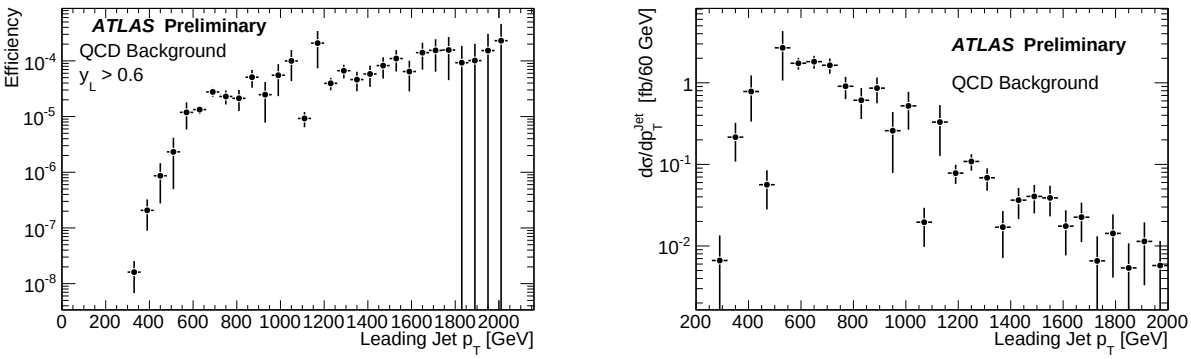

(a) (b)

Figure 12: Total selection efficiency for QCD multijet background (a) and resulting differential cross-section (b) as a function of leading jet p_T requiring $y_L > 0.6$.

the generated $m_{t\bar{t}}$[5].

We have made a semi-quantitative evaluation of the W boson + 2 jets background as follows. The ALPGEN production cross-section for W bosons associated with two light partons with $p_T^{lepton} > 20$ GeV and $p_T^{lightparton} > 300$ GeV is approximately 3 pb (to be compared with 7 pb for lepton+jets $t\bar{t}$ production with one parton above 300 GeV.) Only 10% of these events pass the ΔR(lepton,jet) $<$ 0.6 cut described in section 3.1. The other jet then needs to pass the hadronic top cuts for the event to contribute to the background, a rejection of another factor 10. We conclude that the W boson plus jets background is at least a factor of ten smaller than the irreducible $t\bar{t}$ background and do not consider it further for this study.

$m = 2$ TeV	$y_L > 0.6$	$y_L > 0.9$	$y_L > 1.2$
QCD multijet	1.9 ± 0.5	0.7 ± 0.2	0.16 ± 0.04
SM $t\bar{t}$	$21.9 \pm 1.0 \pm 3.9$	$14.2 \pm 0.9 \pm 2.6$	$4.0 \pm 0.5 \pm 0.7$
Total	23.8 ± 4.1	14.9 ± 2.8	4.2 ± 0.9
$m = 3$ TeV	$y_L > 0.6$	$y_L > 0.9$	$y_L > 1.2$
QCD multijet	0.5 ± 0.2	0.2 ± 0.1	0.07 ± 0.03
SM $t\bar{t}$	$2.9 \pm 0.1 \pm 0.5$	$1.8 \pm 0.1 \pm 0.3$	$0.7 \pm 0.1 \pm 0.1$
Total	3.4 ± 0.6	2.0 ± 0.3	0.8 ± 0.2

Table 1: Selected events in the $m = 2$ and 3 TeV mass windows for different hadronic top monojet likelihood cuts for the dominant backgrounds in 1 fb^{-1} of data. For SM $t\bar{t}$, the first uncertainty is statistical and the second systematic. Uncertainties are added in quadrature in the totals.

	$y_L > 0.6$	$y_L > 0.9$	$y_L > 1.2$
l+jets $Z' \to t\bar{t}$ (2 TeV)	0.094 ± 0.002	0.063 ± 0.002	0.016 ± 0.001
l+jets $Z' \to t\bar{t}$ (3 TeV)	0.136 ± 0.002	0.101 ± 0.002	0.034 ± 0.001

Table 2: Fraction of events in the $m = 2$ and 3 TeV mass windows passing different hadronic top monojet likelihood cuts for the signal samples. The uncertainties given here are statistical only.

To estimate the sensitivity to a narrow resonance decaying to $t\bar{t}$, we use a Bayesian technique that allows us to include uncertainties on the background, signal acceptance and luminosity in the priors.

[5] This is equivalent to re-weighting full simulation signal events to the $t\bar{t}$ continuum background.

We use the DØ experiment's implementation[6)], with a 15% uncertainty on the signal acceptance and a 10% uncertainty on the integrated luminosity. These values are commensurate with estimates used in earlier studies [7]. The results are shown in Table 3. No optimization was done regarding the cut on y_L.

95% C.L. limits on σ x BR($t\bar{t}$) (fb)	$y_L > 0.6$	$y_L > 0.9$	$y_L > 1.2$
$m = 2$ TeV	550	650	1400
$m = 3$ TeV	160	180	450

Table 3: Expected sensitivities in the $m = 2$ and 3 TeV mass windows for different hadronic top monojet likelihood cuts for 1 fb^{-1} of data. Results are given in terms of 95% C.L. limits on the signal production cross-section time branching ratio to $t\bar{t}$ in fb.

6 Conclusion

In this study, new observables are put forward to distinguish boosted semi-leptonic top decays from fake candidates found in the QCD multijet background. Furthermore, we modified and improved the analysis presented in Ref. [1] to allow for better separation of hadronic top monojets from jets originating from light quarks, notably by means of a likelihood variable. Finally, the Z' boson mass is reconstructed by selecting events in which a boosted semi-leptonic top decay and a hadronic top monojet could be identified. This method (based on the identification of high-p_T tops) yields good signal selection efficiency while rejecting most of the QCD multijet background. Expected 95% C.L. limits on signal production cross-sections times branching ratio to $t\bar{t}$ for $m = 2$ and 3 TeV resonances in 1 fb^{-1} of data are given. These are of the order of 550 (160) fb for $m = 2$ (3) TeV Z' bosons. Since the irreducible background is dominant, better sensitivity will come from improving the top quark momentum resolution and using a more advanced limit-setting technique exploiting the shape of the $t\bar{t}$ mass distribution.

References

[1] G. Brooijmans, "High pt hadronic top quark identification," Tech. Rep. ATL-PHYS-CONF-2008-008, CERN, Geneva, Jan, 2008.

[2] GEANT4 Collaboration, S. Agostinelli *et al.*, *Nucl. Instrum. Meth.* **A506** (2003) 250–303.

[3] J. Allison *et al.*, *IEEE Trans. Nucl. Sci.* **53** (2006) 270.

[4] T. Sjostrand, S. Mrenna, and P. Skands, *JHEP* **05** (2006) 026, `arXiv:hep-ph/0603175`.

[5] S. Frixione and B. R. Webber, *JHEP* **06** (2002) 029, `arXiv:hep-ph/0204244`.

[6] S. Frixione, P. Nason, and B. R. Webber, *JHEP* **08** (2003) 007, `arXiv:hep-ph/0305252`.

[7] ATLAS Collaboration, G. Aad *et al.*, `arXiv:0901.0512`.

[8] J. Thaler and L.-T. Wang, *JHEP* **07** (2008) 092, `arXiv:0806.0023 [hep-ph]`.

[9] J. M. Butterworth, B. E. Cox, and J. R. Forshaw, *Phys. Rev.* **D65** (2002) 096014, `arXiv:hep-ph/0201098`.

[10] M. Cacciari and G. P. Salam, *Phys. Lett.* **B641** (2006) 57–61, `arXiv:hep-ph/0512210`.

[6)] http://www-d0.fnal.gov/Run2Physics/limit_calc/limit_calc.html